Effect of Nb2O5 coating on the corrosion resistance of the 7050-T7451 aluminium alloy

Murilo Oliveira Alves Ferreira

Materials Engineering Department, São Carlos School of Engineering, University of São Paulo

https://orcid.org/0000-0003-1694-3583

Gabriella Terezinha Lima Teixeira

Institute of Exact Sciences, Naturals and Education, Federal University of Triângulo Mineiro (UFTM)

https://orcid.org/0000-0001-8620-4773

Natália Bueno Leite

Institute of Exact Sciences, Naturals and Education, Federal University of Triângulo Mineiro (UFTM)

https://orcid.org/0000-0001-5442-1765

Rogério Valentim Gelamo

Institute of Exact Sciences, Naturals and Education, Federal University of Triângulo Mineiro (UFTM)

https://orcid.org/0000-0003-2124-3450

Haroldo Cavalcanti Pinto

Materials Engineering Department, São Carlos School of Engineering, University of São Paulo

https://orcid.org/0000-0002-8007-5832

Idalina Vieira Aoki

Polytechnic School, Chemical Engineering Department, University of São Paulo   https://orcid.org/0000-0002-8203-2625

Jeferson Aparecido Moreto (✉ jamoreto@usp.br)

Materials Engineering Department, São Carlos School of Engineering, University of São Paulo

https://orcid.org/0000-0001-9837-3216

Research Article

Effect of Nb_2O_5 coating on the corrosion resistance of the 7050-T7451 aluminium alloy

M. O. A. Ferreira[1]; G. T. L. Teixeira[1]; N. B. Leite[1]; Gelamo, R. V.[2]; H. C. Pinto[3]; I. V. Aoki[4]; J. A. Moreto[3]*

[1]Institute of Exact Sciences, Naturals and Education, Federal University of Triângulo Mineiro (UFTM). Avenida Doutor Randolfo Borges Júnior, Univerdecidade, 38064200 - Uberaba, Minas Gerais, Brazil.
[2]Institute of Technological and Exact Sciences, Federal University of Triângulo Mineiro (UFTM). Avenida Doutor Randolfo Borges Júnior, Univerdecidade, 38064200 - Uberaba, Minas Gerais, Brazil.
[3]Materials Engineering Department, São Carlos School of Engineering, University of São Paulo, 13563-120, São Carlos, São Paulo, Brazil.
[4]Polytechnic School, Chemical Engineering Department, University of São Paulo, Av. Prof. Luciano Gualberto, travessa 3, 380 Cidade Universitária, São Paulo, São Paulo, Brazil.

*Corresponding author: jeferson_moreto@yahoo.com.br

Abstract

The aircraft industry has been searching for new materials to be used in their aircrafts, which provide good mechanical and corrosive properties. The 7xxx series aluminium alloys are widely used in structural components. However, these alloys are susceptible to localised corrosion processes when exposed to an aggressive environment, which affect their lifetime and performance. Surface treatment appears as a powerful tool to improve the corrosion resistance of these alloys, since the coating may act as a protective physical barrier. This work aims to present an innovative and applied research for the development of the Nb_2O_5 thin films on the 7050-T7451 aluminium alloy surface by using the reactive sputtering technique. The open circuit potential, potentiodynamic polarization, electrochemical impedance spectroscopy as well as immersion tests were used to access the corrosion behaviour of the 7050-T7451 aluminium alloy in 0.6 mol L^{-1} NaCl solution. The morphology of the coated and uncoated specimens was verified by using optical microscopy, AFM and SEM/EDX techniques. Results demonstrated a difference of about 315 mV between the pitting potential ($E_{pitting}$) and corrosion potential (E_{corr}) for the coated material, indicating the positive effect of Nb_2O_5 thin films on the corrosion resistance of the alloy. In addition, EIS results displayed the reactive sputtering technique was advantageous, since the impedance modulus increased significantly.

Finally, the EIS measurements corroborate with the AFM results, showing the Nb_2O_5 coating at the beginning of the corrosion tests is about 300 nm in thickness. To the best of our acknowledgement, this is the first study concerning the improvement of the corrosion properties of 7050-T7451 aluminium alloy by using the methodology presented in this work.

Graphical Abstract
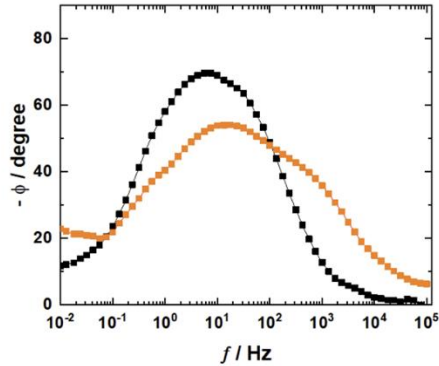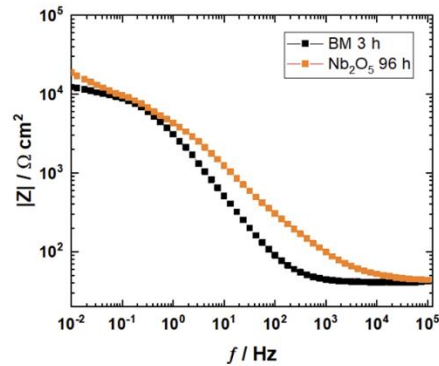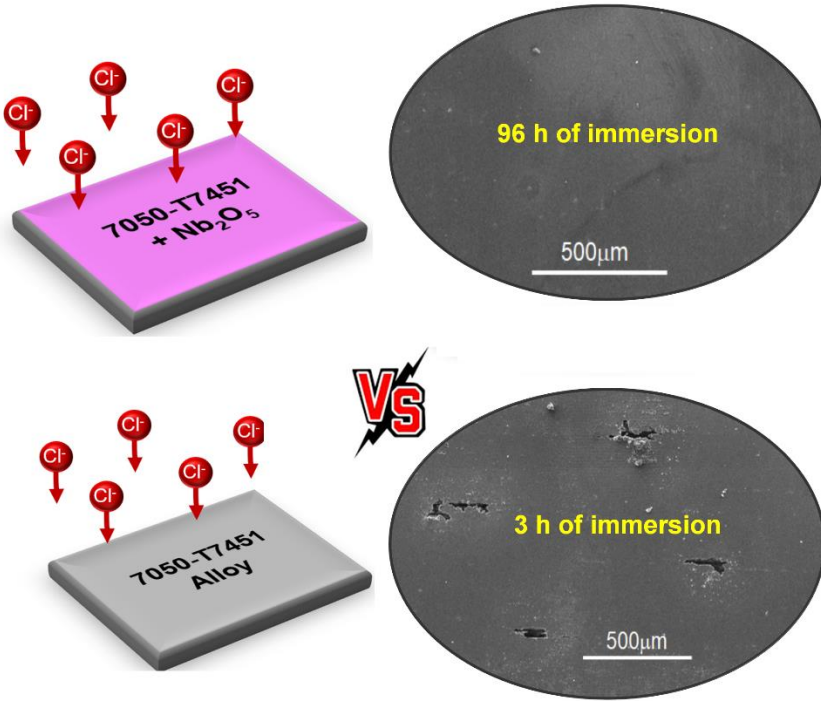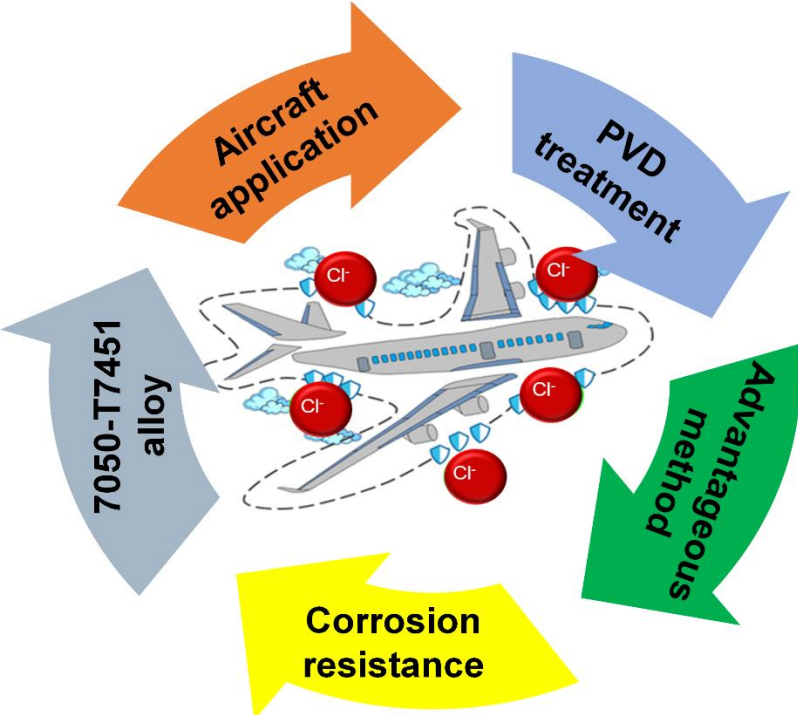
1. Introduction

The aircraft industry has been constantly looking for the development of materials that display good mechanical and corrosion properties, as well as low manufacturing and maintenance costs [1, 2]. Aluminium is widely used in this sector due to its low density, easy malleability, and good resistance to global and localised corrosion processes in an aggressive medium. Relatively pure aluminium exhibits good corrosion resistance due to the formation of Al_2O_3 thin film that spontaneously forms on its surface. The addition of alloying elements, such as: copper (Cu), magnesium (Mg), iron (Fe), manganese (Mn) and zinc (Zn) increase the mechanical properties of aluminium, creating the different series of aluminium [3.4]. Considering the aeronautical and aerospace industry, the 2xxx and 7xxx series are the mostly used.

The 2xxx series alloys have Cu and Mg as main alloying elements and are used as airframe material due to their good fatigue resistance and high damage tolerance. Such properties are conferred mainly by the presence of Cu in the alloy [5, 6]. Regarding the 7xxx series alloys, the main elements are Cu, Mg and Zn. The addition of these elements into the alloy matrix improves its mechanical properties. The formation of different types of second-phase particles is related to the thermal aging processes [7, 8]. The intermetallics (IMs) on aluminium alloys may be classified as follows: primary particles that are responsible for increasing the mechanical properties of the material (also named as strength precipitates) as well as the second-phase particles, which can be incoherent or semi-coherent with the metallic matrix and are harmful to the global and localised corrosion processes. As reported by the literature [9, 10], the formation of primary particles on 7xxx series aluminium alloys follows four stages, namely: (i) solid supersaturated solution, (ii) Guinier-Preston zones (GP zones), (iii) η' and (iv) η phases (MgZn$_2$) [9,10]. The determining factor for the successful formation of these particles is closely linked to the Zn/Mg ratio [11]. As already mentioned, primary particles are responsible for increasing the mechanical properties of the 7xxx series aluminium alloys [12]. On the other hand, the formed particles due to the precipitation process are related to a reduction in the corrosive properties of the 7xxx series.

In general, different factors related to the microstructure of the 7xxx series alloys influence their mechanical and corrosive properties [12-14]. Song and collaborators [15] highlighted that the microstructure of the 7050-T7451 aluminium alloy is composed of different regions, namely: (i) recrystallized grains, (ii) non-recrystallized structure of sub-grains, (iii) different types of primary precipitates, (iv) η and η' phases as

4

well as (v) different second phase particles (Al_2CuMg and Al_7Cu_2Fe) [11,16,17]. Second-phase particles arise from precipitation processes in the 7xxx series alloys [18]. As mentioned by Song and colleagues [17], the main second-phase particles found in 7050-T7451 aluminium alloy are $MgZn_2$ and Al_7Cu_2Fe phases, respectively. The Al_2CuMg phase displays a lower volumetric density when compared to the others and, for this reason, it is not possible to ensure its specific influence on corrosion processes of 7xxx series aluminium alloys [19].

As reported by Yu et al [20], grain boundaries are the regions most susceptible to the corrosion process on 7050-T7451 aluminium alloy, leading to the formation of pitting and, consequently, reducing the fatigue life of the material [21]. In fact, pits act as stress concentrators and directly affect the fatigue life of a mechanical component. Likewise, the presence of incoherent and coherent second-phase particles in regions close to grain boundaries accelerates the localised corrosion process [18]. Furthermore, Sun et al [21] pointed out that, for 7050-T7451 aluminium alloy, the potential difference between the aluminium matrix and the Al_7Cu_2Fe second-phase particle is approximately 410.8 mV. Moreto et al [4] presented comparative studies related to global and localised corrosion processes 7050-T7451 and 7081-T73511 aluminium alloys in an aggressive medium containing chloride ion. For this purpose, open circuit potential, potentiodynamic polarization curves, electrochemical impedance spectroscopy, SVET (Scanning Vibrating Electrode Technique), and SKP (Scanning Kelvin Probe) techniques were used. Results demonstrated the 7050-T7451 and 7081-T73511 aluminium alloys present a very similar corrosive behaviour, which may be directly related to the galvanic coupling of the second-phase particles and the metallic matrix. With respect to the mechanical properties, the 7050-T7451 aluminium alloy exhibited higher values of tensile strength and yield strength (σ_{YS}) when compared to 7081-T73511 alloy [24, 25]. These findings only confirm the good mechanical and corrosive properties of the 7050-T7451 aluminium alloy.

It is known that the main exposure region of an aircraft is the saline environment, whether during flight or when stopped at airports that are located close to coastal regions. It is also verified that there is an increase in the corrosive processes of aircraft due to the presence of the seawater fog in these environments [4, 15, 20, 24, 26, 27]. The use of coatings on the 7050-T7451 aluminium alloy surfaces appears as a powerful strategy, since these coatings act as a protective physical barrier, preventing the contact of aggressive ions with the base material and, therefore, increasing the corrosion

properties of aluminium alloys. Diamond-like Carbon (DLC) thin films have been widely used by the industrial sector due to their relatively high hardness, good resistance to abrasive processes, low coefficients of friction, and chemical inertness [28-31]. However, DLC films deposited by using the sputtering technique have different types of defects inherent to their manufacturers, such as flaws or pores, delamination, and film fragmentation. In this way, researchers have sought the development of materials that present significant improvements in these properties.

Recent studies show the versatility of niobium pentoxide (Nb_2O_5) thin films and their applications in different sectors [32-37]. Among these properties, the following stand out: good chemical stability, good adhesion to surfaces and good resistance to corrosion in acidic and alkaline media [38,39]. Among the different types of niobium oxides, the Nb_2O_5 is the one that presents the best mechanical and corrosive properties [40, 41], and can be obtained by using the reactive sputtering technique [32-37] at room temperature. Despite all the advantages of Nb_2O_5 coatings, there are no studies in the literature that consider the influence of Nb_2O_5 thin films on the corrosive properties of 7050-T7451 aluminium alloy. Here, we present an innovative and applied work to verify the influence of Nb_2O_5 thin films deposited by using the reactive sputtering technique on global and localised corrosion processes of 7050-T74511 aluminium alloy in a medium containing 0.6 mol L^{-1} NaCl solution. Finally, it is expected to collaborate with the development, modification, and application of new materials to be used on the aeronautical sector.

2. Experimental 34999114301

2.1. Material

In the present study, the 7050-T7451 aluminium alloy was used with dimensions of 1.5 cm x 1.5 cm. The chemical composition (wt%) of the mentioned alloy is 2.25 Cu, 0.04 Si, 0.05 Fe, 1.9 Mg, 0.01 Mn, 0.03 Ti, 0.1 Zr, 6.02 Zn, 0 .01 Cr, and Al as balance. Before the deposition of Nb_2O_5 coatings by using the reactive sputtering technique, the 7050-T74511 aluminium alloy was sanded with silicon carbide (SiC) sandpaper in the sequence of 800, 1200, 2400, and 4000 mesh, respectively. After, the polishing process was performed with diamond paste in the sequence of 3, 2, and 1 μm. Subsequently, the samples were washed in distilled water and placed in ultrasound with isopropyl alcohol for a period of 10 min. After the washing process, the specimens were dried using air jets and conditioned in a desiccator for further analysis.

2.2. Obtaining Nb_2O_5 coatings on the 7050-T7451 aluminium alloy surfaces by using reactive sputtering technique

The Nb_2O_5 thin film deposition methodology has already been established by this research group and can be found in detail in the following references [32-37]. However, a basic description is presented in this work to situate the reader. Nb_2O_5-based coatings were deposited on the surface of the 7050-T7451 aluminium alloy by using reactive sputtering technique at room temperature without additional post deposition treatment. The deposition system is composed by a magnetron sputtering purchase from Kurt Lesker Co. for targets of 2.0 inches diameter. The vacuum is supported by rotative and turbomolecular pumps allowing pressure of 0.001 mTorr. Gases were admitted and controlled by needle valves from Edwards Co. The film depositions were conducted at 5.0 mTorr using Argon (99.999% White Martins). To obtain Nb_2O_5 stoichiometry films, O_2 (99.999% White Martins) at 0.5 mTorr was used. Furthermore, the DC voltage and current used was about 450 V and 145 mA, respectively. Finally, the thickness of the Nb_2O_5-based coatings produced in the present survey is around 250 to 300 nm.

2.3. Morphological and structural characterization of the Nb_2O_5-based coatings

Nb_2O_5-based coatings produced by using reactive sputtering technique have already been extensively characterized via X-ray diffraction (XRD) and the Rietveld method, Fourier-transform infrared spectroscopy (FTIR), Raman spectroscopy and X-ray photoelectron spectroscopy in previously published works [32-37]. In this sense, the structural characterization of the coating will not be presented in this study. However, the morphology of the 7050-T7451 and 7050-T7451/Nb_2O_5 was evaluated before and after the corrosion tests as ascribed in the next sections. For this purpose, scanning electron microscopy (SEM) micrographs were assessed through an analytical FEG- SEM JEOL 7001 F equipped with an Oxford light elements EDX detector. Optical images were obtained after the corrosion tests using an Olympus BX60M optical microscope with a high-resolution digital camera (5.0 Megapixels). The AFM results were obtained in a Shimadzu SPM9700 microscopy using dynamic mode and cantilevers purchase from NT-MDT Co.

2.4. Electrochemical assays

In the present work, three corrosion tests were carried out: open circuit potential (OCP), potentiodynamic polarization (PP), and electrochemical impedance spectroscopy (EIS). The corrosion potential (E_{corr}) of the 7050-T7451 and 7050-T7451/Nb_2O_5 samples was monitored during 10,800 s (3h). After the potential stabilization, the last measured value was used to determine the potential window for carrying out the PP tests. The PP tests were performed with a potential window of $\pm$ 500 mV from E_{corr}, using a sweep rate of 0.5 mVs^{-1}. Through the PP tests it will be possible to characterize the anodic and cathodic domains as well as determine the value of the pitting potential ($E_{pitting}$) for the coated and uncoated 7050-T7451 aluminium alloy.

The EIS tests were performed to evaluate the properties of the Nb_2O_5-based coatings deposited on the 7050-T7451 aluminium alloy surfaces by using reactive sputtering technique. The EIS tests were performed at increased immersion times of the 3, 10, 15, 24, 48 and 96 h, respectively. The EIS spectra were obtained in the frequency range from 100 kHz to 10 mHz with 8 points/decade. An electrical equivalent circuit (EEC) was proposed to adjust EIS data, using the *Zview2 software*. As is known, for aluminium alloys in chloride media the pitting potential ($E_{pitting}$) and the corrosion potential (E_{corr}) are nearly the same [4]. In this way, a small displacement of the potential values above E_{corr} will lead to the beginning or the propagation of pitting, causing an increase in the electric current density values and, therefore, resulting in non-linearity and invalidating the EIS measurement. For this reason and following the recommendations of Mansfeld and Fernandes [40], the EIS tests were carried out at 20 mV negative to E_{corr} using an applied a.c. signal of 10 mV (rms).

All electrochemical tests were conducted in a naturally aerated solution (0.6 mol L^{-1} NaCl) at room temperature, using a μStat-i-400s Bipotentiostat/galvanostat and a classical three-electrode configuration: working electrode (WE) consisting of 7050-T7451 and 7050-T7451/Nb_2O_5 specimens, platinum as a counter-electrode (CE), and saturated calomel electrode as reference (SCE) Hg/Hg_2Cl_2, KCl$_{sat}$. The working electrodes (coated and uncoated) presented an area of testing about 1 cm^2.

2.5. Immersion tests

Immersion tests were performed on uncoated and coated 7050-T7451 aluminium alloy during 96 h of immersion in 0.6 mol L^{-1} NaCl solution. After the end of the tests, the specimens were properly washed by using distilled water during 10 min. The coating was produced on the top surface of the specimens. So, on the immersion tests, the other areas were isolated with beeswax. All morphological surfaces were accessed via optical microscopy (Nova 156-T optical microscope with a high-resolution digital camera (5.0 Megapixels). SEM micrographs were also obtained through an analytical FEG- SEM JEOL 7001 F equipped with an Oxford light elements EDX detector.

3. Results & Discussion

Figure 1 (a) exhibits the 3D microstructural characteristics of the 7050-T7451 aluminium alloy obtained via OM technique. A very intense lamination process may be observed as well as elongated grains in the short – longitudinal (SL) and longitudinal-transverse (LT) planes, respectively. In addition, the presence of non-metallic inclusions distributed throughout the aluminum matrix (small black dots) can be verified. **Figure 1 (b)** shows the micrograph obtained via SEM of the 7050-T7451 aluminium alloy in the top direction. The microstructure of the 7050-T7451 alloy is composed of a solid aluminum solution and submicrometric second-phase particles distributed along the metal matrix. The yellow dotted line in **Figure 1 (b)** shows a continuous arrangement of the second-phase particles as well as the magnification of a given region.
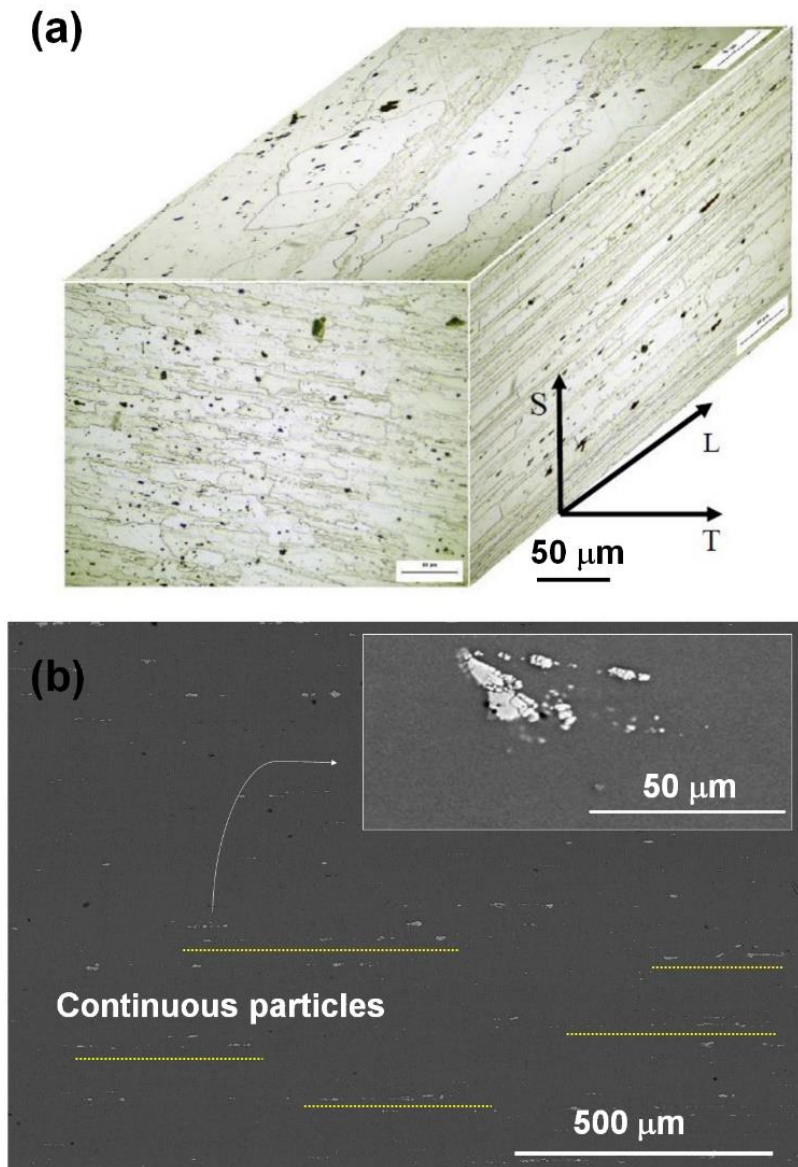
Figure 1. (a) 3D microstructural characteristics of the 7050-T7451 aluminium alloy obtained via OM technique and **(b)** low magnification SEM image of the 7050-T7451 aluminium alloy in the top direction, showing distribution of second-phase particles. The image located at the top right displays details of an agglomerate of second-phase particles. Image obtained with combined BSD + SE modes.

A schematic assembly obtained by using OM technique at different magnifications for the 7050-T7451 and 7050-T7451/Nb$_2$O$_5$ aluminium alloy after 96 h of immersion in a 0.6 mol L^{-1} NaCl solution may be seen in **Figure 2**. Results demonstrated a very intense corrosion process (see **Figure 2 (a)**), presenting regions of severe localised corrosion (**Figure 2 (b)**) for the base material. **Figure 2 (c)** clearly exhibits the formation of pitting on the 7050-T7451 aluminium alloy surface. These findings are probably

directly related to the preferential dissolution process of the 7050-T7451 metallic matrix and will be discussed in detail in the next sections with the aid of the SEM/EDX techniques. The localised corrosion process on 7050-T7451 aluminium alloy is due to the galvanic coupling of the second-phase particles with the aluminium matrix. Studies previously published by Moreto et al [4] displayed the cathodic behaviour of the Al_7Cu_2Fe second-phase particle. In other words, during the immersion tests, the Al_7Cu_2Fe particle presents a nobler potential when compared to the aluminium matrix, promoting a preferential dissolution process on its surrounding. As these particles are distributed along the entire length of the aluminum matrix, several regions of localised corrosion are formed. With respect to the coated material, the Nb_2O_5 thin film deposited on the 7050-T7451 aluminium alloy surface by using reactive sputtering technique acts as a protective barrier, preventing the progress of the localised corrosion process (see **Figures 2 (d-f)**). Previous studies carried out by this research group have already shown the protective effect of Nb_2O_5 thin films on the corrosion protection of 2524-T3 [35] and 2198-T851 [32, 33] aluminium alloys as well as Ti-6Al-4V alloy [34]. For the same time interval (96 h of immersion of 0.6 mol L^{-1} NaCl) the coated material presents a much more intact surface when compared to the base material. These initial results are totally motivating and manage to show in a very general way the protective effect of the Nb_2O_5 coating.

Figure 3 exhibits the surface morphology of the 7050-T7451 aluminium alloy after the immersion tests. Here, 100 x magnification SEM image obtained by using back-scattered electrons (BSD) mode of 7050-T7451 aluminium alloy is presented in **Figure 3 (a)**, which shows various attacked regions along the metal matrix. The presence of corrosion products may be seen in a magnified region as demonstrated in **Figure 3 (b)**, whilst the EDX spectrum obtained from the highlighted region are represented in **Figures 3 (c, d)**, which primarily indicate the presence of Al and O elements, respectively. As is already well established for aluminium, this observation suggest dissolution of the 7050-T7451 matrix and precipitation of aluminium hydroxide, $Al(OH)_3$, forming amorphous domes on the top surface.

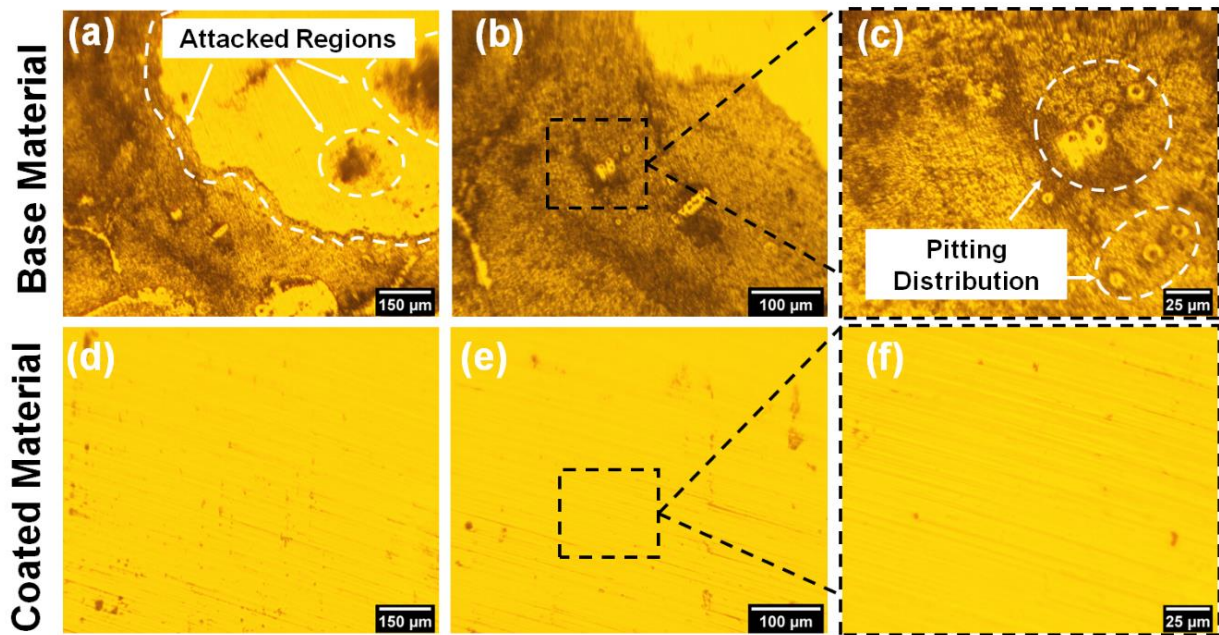**Figure 2**. Images obtained by using OM technique at different magnifications for the 7050-T7451 and 7050-T7451/Nb_2O_5 aluminium alloy after 96 h of immersion in a 0.6 mol L^{-1} NaCl solution. **(a)** 10x, **(b)** 20x, and **(c)** 50x.
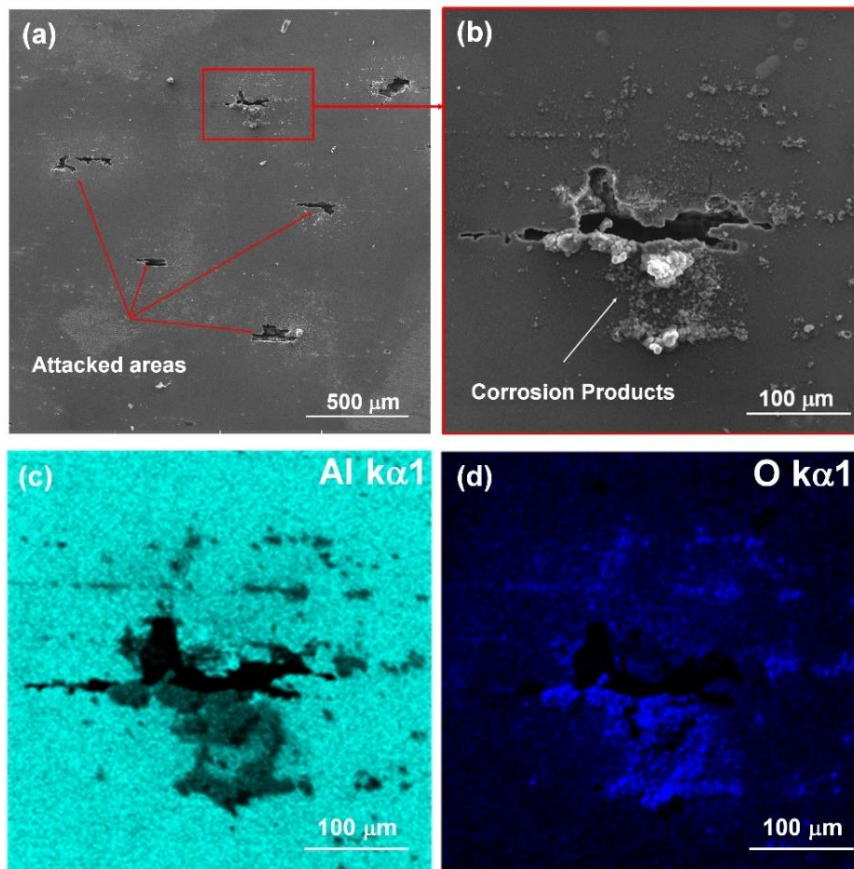

Figure 3. SEM images **(a, b)** and EDX maps **(c, d)** for the 7050-T7451 aluminium alloy after 96 h of immersion in a 0.6 mol L^{-1} NaCl solution.

Figure 4 shows the morphology of corrosion damage that occurs upon coated 7050-T7451 aluminium alloy following immersion in 0.6 mol L^{-1} NaCl solution for a period of 96 h. The results clearly show the positive influence of Nb_2O_5 coatings as a protective physical barrier against the corrosion process. While the base material showed a severe corrosion process over the entire surface, the coated-7050-T7451 aluminium alloy exhibited the formation of a single pit as shown in **Figures 4 (a)** and **4 (b)**, respectively. The EDX maps (see **Figures 4 (c-e)**) demonstrate the absence of Nb element on the highlighted region as well as the presence of Al and O, respectively. Probably, aggressive ions (Cl^-) permeated through the coating defect, initiating a localised corrosion process. Moreto et al [35], pointed delamination-like events as well as propagation of corrosion process beneath the Nb_2O_5 thin film, promoting the coating detachment for the 2524-T3 aluminium alloy. However, in the present work, no delamination process was verified. These observations indicate that 7050-T7451 aluminium alloy has a different corrosion mechanism when compared to the 2524-T3 alloy.
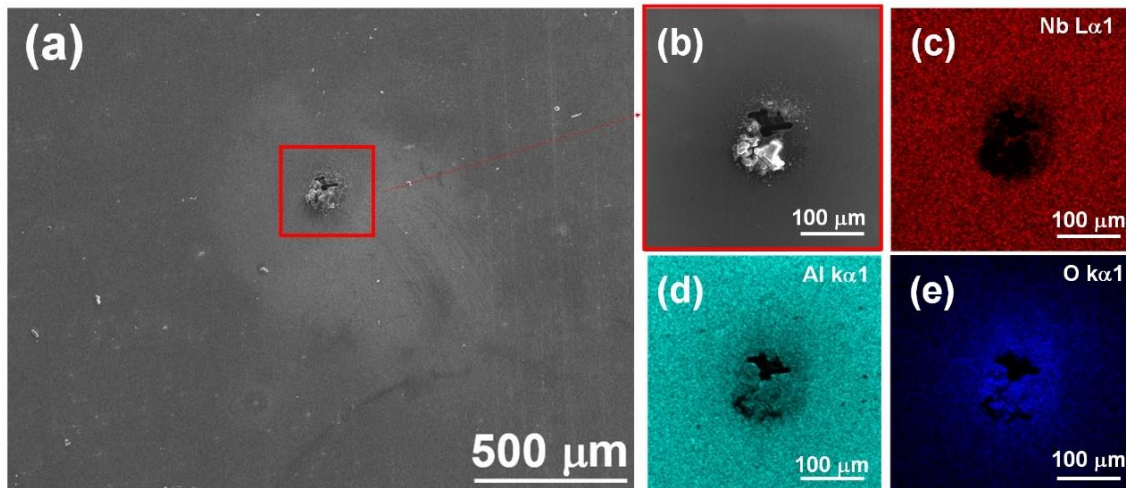

Figure 4. SEM images **(a, b)** and EDX maps **(c- f)** for the 7050-T7451 aluminium alloy containing Nb_2O_5 thin film after 96 h of immersion in a 0.6 mol L^{-1} NaCl solution.

The OCP values of the coated and uncoated 7050-T7451 aluminium alloy were monitored for 10,800 s (3 h) in 0.6 mol L^{-1} NaCl solution as presented in **Figure 5 (a)**. It can be verified that both materials present a very similar behaviour. A preliminary analysis of the OCP curves based on the potential corrosion (E_{corr}) would suggest that both materials have the same thermodynamic stability in solution containing chloride ions. **Figure 5 (b)** shows the PP curves for the uncoated and coated 7050-T7451 aluminium alloy. The results demonstrated that no passive plateau may be observed in

the anodic domain of the 7050-T7451 aluminium alloy, as current sharply increases due to immediate growth of pits, indicating that pitting naturally occurs at the corrosion potential ($E_{ocp} \sim - 0.71$ V SCE). The value of E_{corr} is normally seen as an indicative of the nobility of the material, a higher E_{corr} corresponding to a more corrosion resistant system. In this sense, a preliminary result would indicate that the 7050-T7451 aluminium alloy containing the Nb_2O_5 thin film is more prone to corrosion. However, it is very important to note that the pitting potential ($E_{pitting}$) values were nearly the same for both conditions. Moreover, the large difference observed, for the coated specimens, between the E_{corr} and the $E_{pitting}$, i.e., about 315 mV, could be seen as margin of safety, guaranteeing that $E_{pitting}$ will not be attained. Freitas and collaborators [32] studied the corrosion behaviour of reactive sputtering deposition niobium oxide-based coating on the 2198-T851 aluminum alloy and verified a difference about 210 mV between the $E_{pitting}$ and E_{corr}. Another interesting result that should be mentioned in this work was proposed by Moreto et al [35]. In the mentioned work, the authors focused on the surface modification of 2524-T3 aluminium alloy by using reactive sputtering technique and verified a difference about 400 mV between the $E_{pitting}$ and E_{corr}. All these results only indicate the good properties of the Nb_2O_5 thin film in protecting aluminium alloys.

In the present survey, EIS tests were carried out to evaluate the corrosion resistance, under stationary conditions, of the uncoated and coated 7050-T7451 aluminium alloy. The Bode plots for the coated and uncoated samples immersed in 0.6 mol L^{-1} NaCl solution during 3, 10, 15, 24, 48 and 96 h are presented in **Figure 6 (a)** and **6 (b),** respectively. A comparison between 3 and 96 h of immersion times for coated and uncoated materials is shown in **Figure 6 (c)**. An overview of the spectra shows the presence of two-time constants: one at high frequencies that corresponds the presence of oxide film and another at low frequencies and which is related to localised corrosion processes. In fact, as expected, the coated 7050-T7451 alloy exhibited higher values of impedance moduli, indicating that the surface treatment improved the corrosion properties of the 7050-T7451 aluminium alloy in the chloride-containing medium (see **Figure 6 (c)**). Based on the EIS tests shown in **Figure 6**, an equivalent electrical circuit (EEC) (see **Figure 7**) has been used to explain the corrosion behaviour of the uncoated and coated 7050-T7451 aluminium alloy.
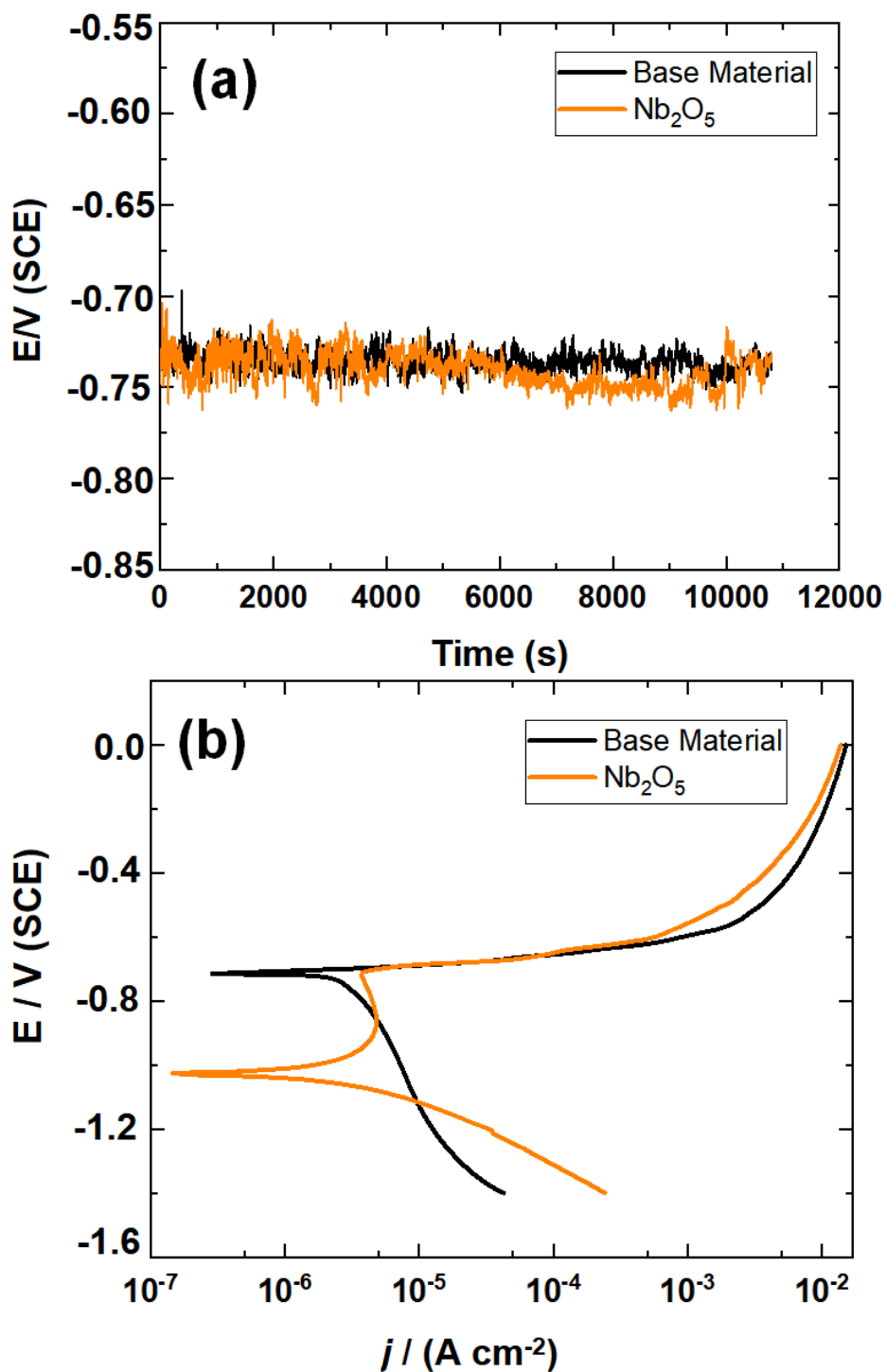
Figure 5. **(a)** OCP measurements and **(b)** PP curves for the 7050-T7451 aluminium alloy uncoated and coated with Nb_2O_5 thin film in aerated 0.6 mol L^{-1} NaCl aqueous solution at scan rate of 0.5 mV s^{-1}. All measurements were performed in triplicate and showed good reproducibility.
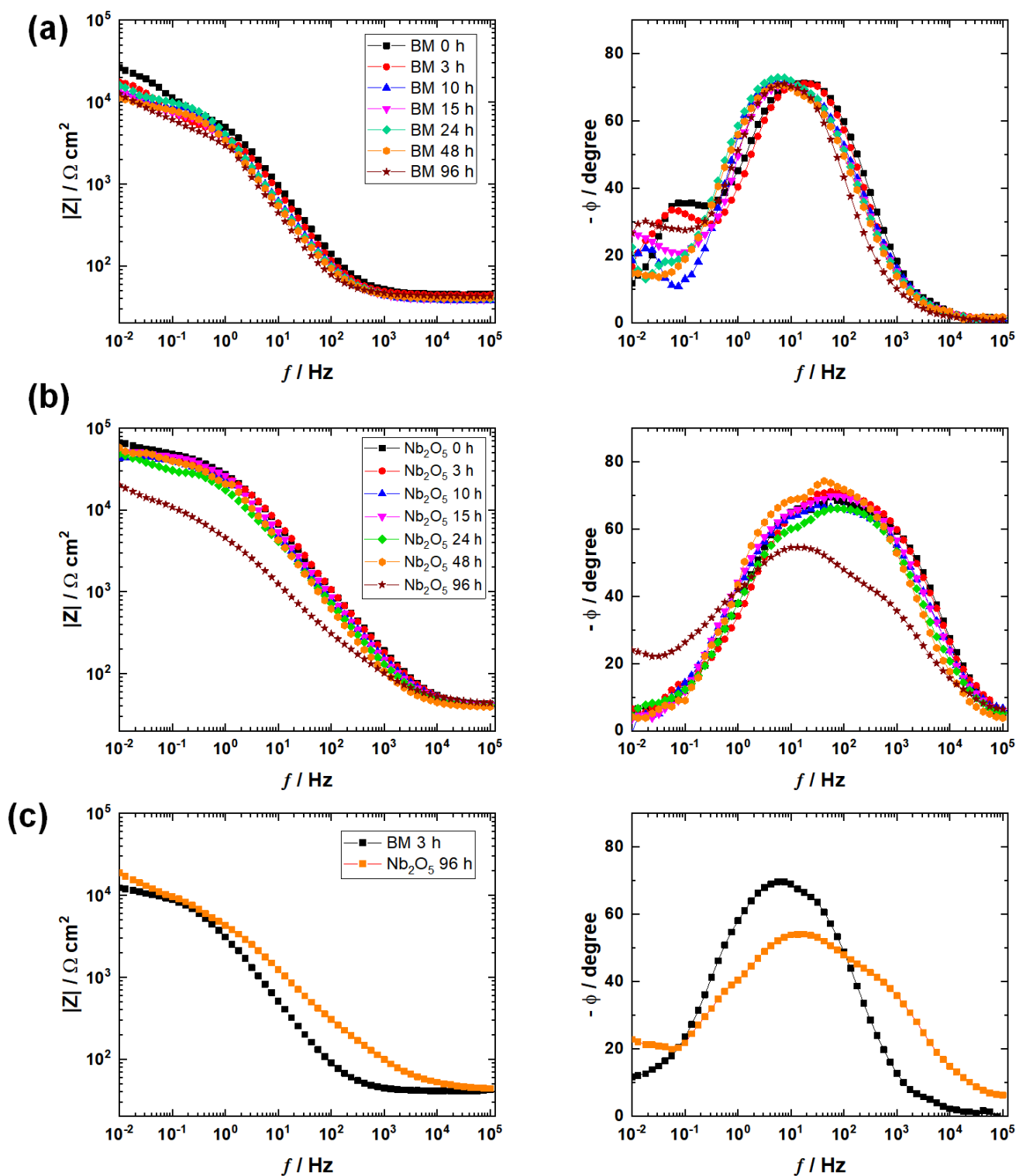
Figure 6. EIS spectra (Bode plots) of **(a)** base material, **(b)** Nb$_2$O$_5$-coated 7050-T7451 aluminium alloy exposed to 0.6 mol L^{-1} NaCl solution and **(c)** a comparison between 3 and 96 h of immersion times for coated and uncoated materials.
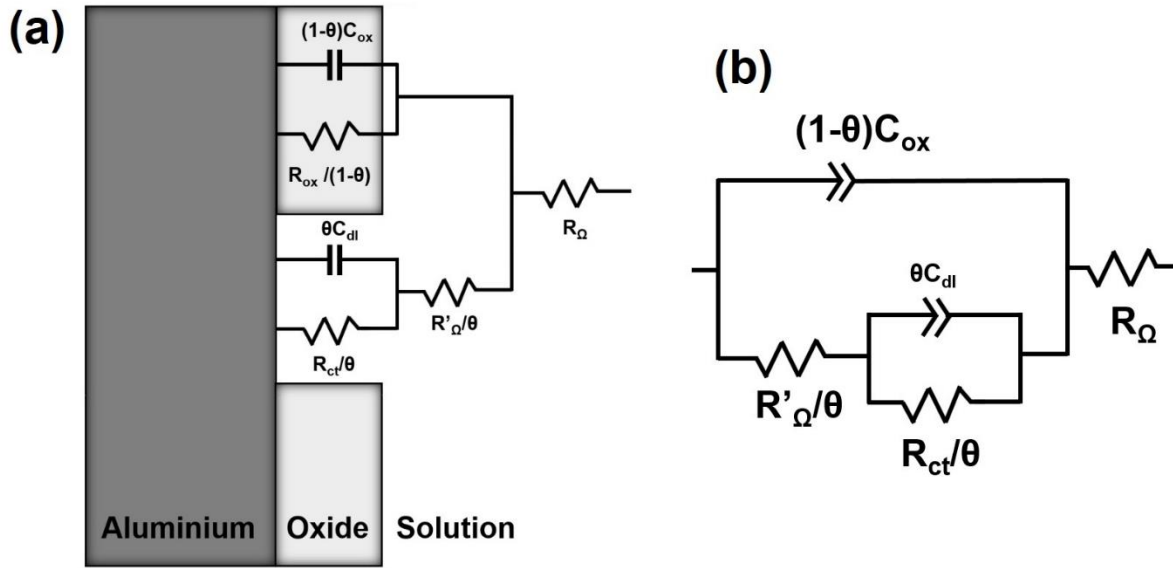
Figure 7. (a) Corresponding EEC used to fit the EIS data for coated and uncoated 7050-T7451 aluminium alloy in 0.6 mol L^{-1} NaCl medium, and **(b)** EEC used for fitting the experimental data.

Several authors have proposed ladder equivalent circuits like the one shown in **Figure 7 (a)** to account for the behaviour of localised corrosion in aluminium alloys, especially those of series 2XXX and 7XXX [4, 32, 35, 41, 42]. Here, the EEC is composed by the contribution of the pitting process that occurs in an area fraction θ as well as the remaining oxide film, which occupies an area fraction $(1-\theta)$. The R_{ct}–C_{dl} network represents the charge transfer reaction corresponding to the localised corrosion and the capacitance of the double-layer. As can be seen in the EEC representation, the R_{ct}–C_{dl} loop is associated to the additional resistance of the electrolyte inside the pit/pore, R'_{Ω}. The R_{ox}–C_{ox} loop is related to the electrical resistance and the dielectric capacitance of the oxide layer, respectively. Finally, the solution resistance may be represented by R_{Ω}, and is added to this parallel association.

As is known, aluminium and its alloys spontaneously form a thin film of alumina (Al$_2$O$_3$) on their surface when exposed to the environment. In the case of insulating oxides, such as Al$_2$O$_3$, in the base material, or Nb$_2$O$_5$, in the coated one, the R_{ox} parameter exhibits an extremely higher value. In this sense, there is a poor conduction of electrons inside the oxide film and the R_{ox} term may be removed from the EEC presented in **Figure 7 (a)**. Thus, the EEC used for fitting the experimental data may be verified in **Figure 7 (b)**. The capacitors have been replaced by constant phase elements (CPE) to accounting

to the non-ideal behaviour of the system. The impedance of a CPE is given by **equation 1** [43].

$$Z_{CPE} = \frac{1}{Y_0 (j\omega)^n} \tag{1}$$

where the admittance Y_0 and the exponent n are the characteristic parameters. It is important to mention, for $n = 1$ an ideal capacitor behaviour may be verified. The impedance spectra were fitted to this circuit, resulting in a very good correlation, with $\chi 2$ values in the range of 10^{-4}. The average values of the EIS parameters of 7050-T7451 and 7050-T7451/Nb_2O_5 specimens may be verified in **Figure 8**. It is important to point out that only the values of 3, 15 and 96 h of immersion were presented. In fact, a very different behaviour was verified for these immersion times and the explanations will be given in the following paragraphs.

In general, the $R\Omega$ values of both materials remained very close. This observation indicates that the distance between the working and reference electrodes remained constant during the electrochemical tests (see **Figure 8 (a)**)[4, 44]. As already discussed by Moreto et al [45] ,Y_0 parameter do not represent real capacitances values and the conversion of CPE parameters to capacitance values is scarce. On the other hand, the models presented in the literature contemplate quite simple systems in which the existence of only one time constant is verified [46-48]. Here, at first, only a comparison between the behaviour of coated and uncoated alloy will be made, i.e., the CPE's parameters will be considered as capacitances. **Figure 8 (b)** displays the CPE-ox behaviour for the coated and uncoated specimens, indicating an increase of the corroded area with the immersion time. The same behaviour was verified for the CPE-dl parameter (see **Figure 8 (c)**), except for the immersion time of 15 h. The decrease of CPE-dl values for the mentioned time may be attributed to the formation of a surface layer of corrosion products which ends up sealing some very active regions on the specimen surfaces. As can be seen in **Figure 8 (d)**, R_{ct} values display a tendency towards lower values as the immersion time increases. These observations are directly linked to the increase of pitted area, growth of pits as well as acidification of inner pitting. Considering the immersion time of 96 h for the base material, the increase of R_{ct} values is due to the formation of corrosion products on the alloy surface, which partially blocks the pits. Finally, the

highest R'$_\Omega$ values indicate the positive effect of the Nb$_2$O$_5$ thin films to improve the corrosion properties of the 7050-T7451 aluminium alloy.

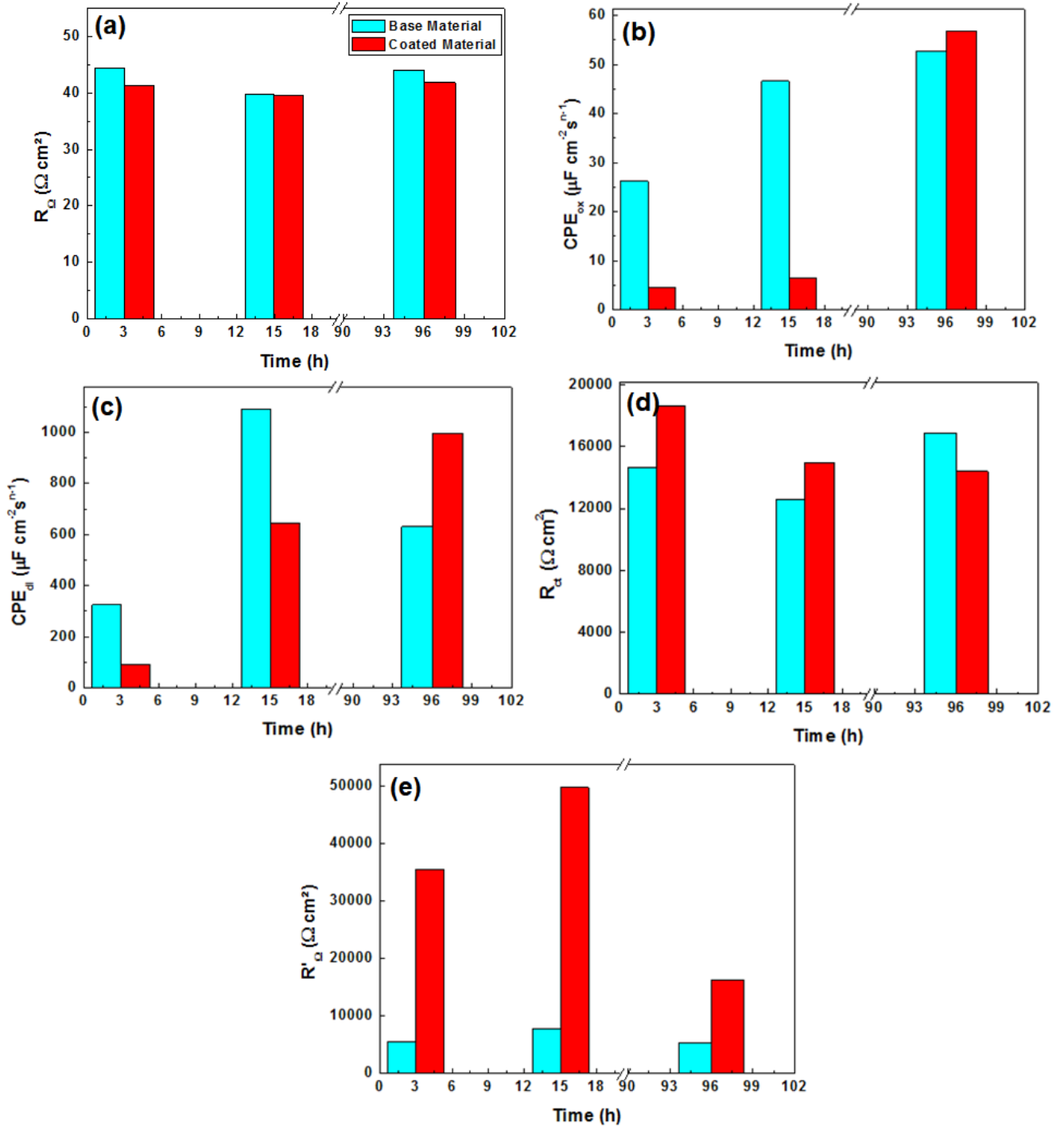**Figure 8.** Average values of the EIS parameters of 7050-T7451 aluminium alloy. **(a)** R$_\Omega$ *versus* t, **(b)** CPE-ox *versus* t, **(c)** CPE-dl *versus* time, **(d)** R$_{ct}$ *versus* time, and **(e)** R'$_\Omega$ *versus* t.

In the present work, the conversion of the CPE-ox to capacitance values was based on the Brug's equation [46] (see **Equations 2**) and was already presented by the authors [32].

$$C_{ox} = \left[Y_{0,ox} \times R_{\Omega}^{(1-n)} \right]^{\frac{1}{n}}$$

(2)

Considering a parallel plate capacitor, the relationship between the thin film thickness and capacitance may be written as:

$$C = k\,\varepsilon_0 A/d$$

(3)

where ε_o is the permittivity of free space (8.854×10^{-12} F/m), k is the relative permittivity of dielectric material, d is the separation between the plates and A is the area of plates. As reported by the literature [49], the relative permittivity of Al_2O_3 is about 9.0 for the dry oxide and 40 for a partially hydrated layer. In contrast, the dielectric constant values of the Nb_2O_5 oxide are about 30-90 [50]. In this sense, it can be verified that the Nb_2O_5 coating displays a thickness of approximately 286 nm for a time of 3 h immersion. This value was determined by using the dielectric of material equal to 35. The behaviour of C_{ox} as function of immersion time is presented in **Figure 9 (a)**, which demonstrates the thickness of the Nb_2O_5 coating at the beginning of the corrosion tests is about 300 nm. **Figure 9 (b)** shows the AFM image illustrating the thickness step at interface between the substrate and Nb_2O_5 film and **Figure 9 (c)** the profilometer values in two regions indicated by traces 1 and 2 in **(b)**. The results obtained by using AFM technique corroborate those obtained by EIS tests. In this sense, if the spontaneous alumina layer formed on the base material is approximately 2 nm thick, a value of approximately 286 nm was expected for the coating. Given the small thickness of the alumina when compared to the Nb_2O_5 coating, the proposed circuit considered only one oxide layer.

Figure 10 shows the surface morphology of the uncoated 7050-T7451 aluminium alloy after the EIS tests. As can be seen in **Figures 10 (a-c)**, there was corrosive attack along the entire surface of the alloy (**Figure 10 (a)**), presence of cracks and a dissolution process around the second-phase particle (**Figure 10 (b)**) as well as the presence of mud-crack pattern on the alloy surface (**Figure 10 (c)**). In addition, it was possible to verify the formation of a dense thin film on the aluminium surface. The presence of Al and O elements were identified by using EDX technique (see **Figure 10 (d)**), indicating the presence of Al_2O_3 film. Analyses were performed at points Z1 and Z2, respectively. As the spectra are very close, only the Z1 region was presented herein. A schematic drawing

showing in detail the second-phase particle on the 7050-T7451 aluminium matrix as well as the EDX spectra may be seen in **Figure 11**.
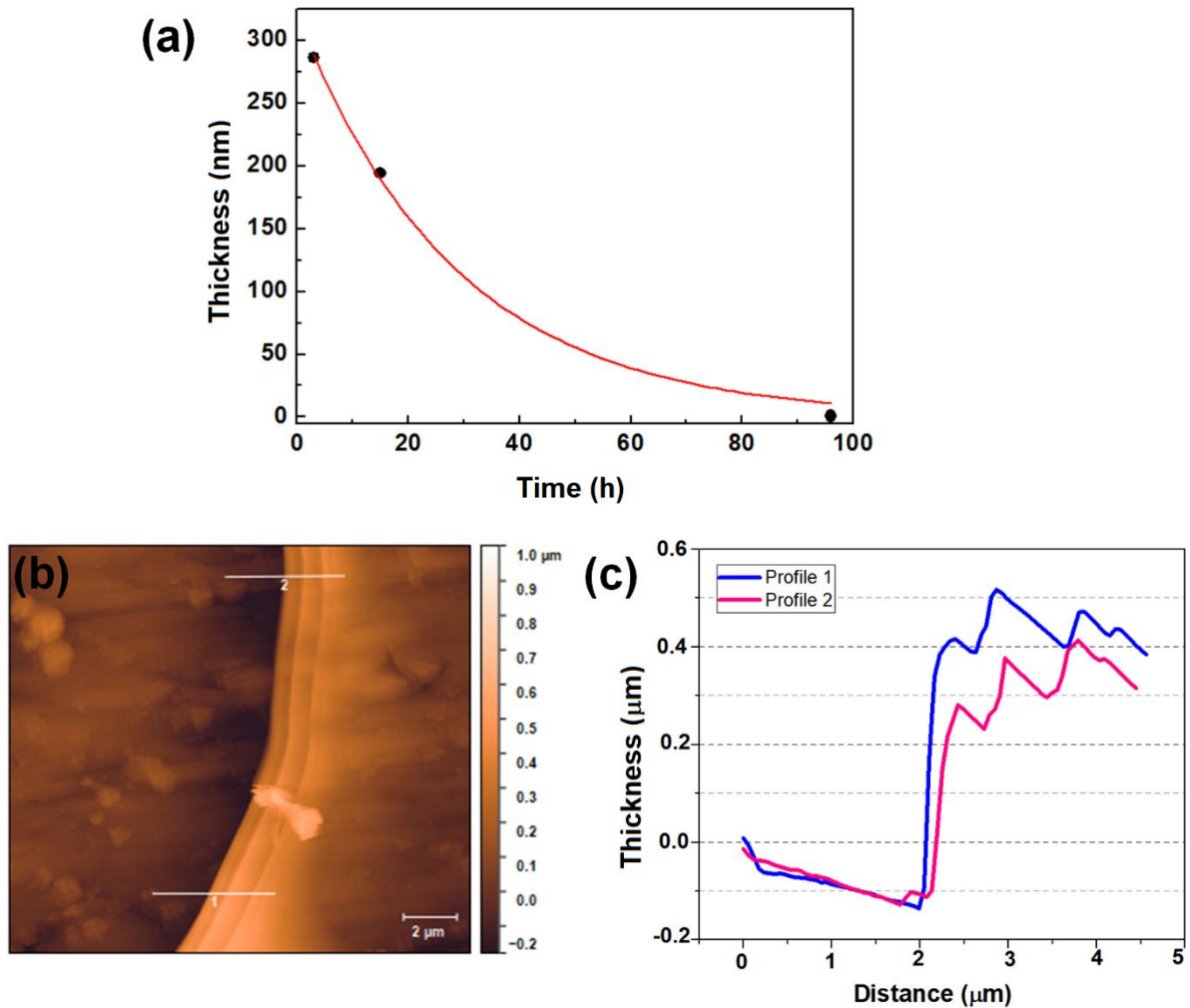

Figure 9. (a) Effect of corrosive medium on the thickness of Nb_2O_5 thin films at different immersion times. **(b)** The AFM image illustrating the thickness step at interface between the substrate and Nb_2O_5 film and **(c)** the profilometer values in two regions indicated by traces 1 and 2 in **(b)**.

The results demonstrated the Al_7Cu_2Fe may serve as a local cathode in the evolution of localised corrosion process. Many researchers [51-55] demonstrated the iron-rich second-phase particles have Volta potential maxima relatively to the aluminium matrix. The effect of the Nb_2O_5 coatings after EIS tests on the protection of 7050-T7451 aluminium alloy in a medium containing aggressive ions can be verified in **Figure 12**. There is a distinct difference between the surfaces of the base and coated materials. In other words, although the presence of pits on the functionalized surface may be verified,

its volumetric density and corrosive attacks are much less intense, demonstrating the protective effect of the Nb_2O_5 coating to improve the corrosion resistance of the 7050-T7451 aluminium alloy. So, in general, this work brings new insights into the effect of the Nb_2O_5 coatings obtained by using reactive sputtering technique on improving the corrosive properties of 7050-T7451 aluminium alloy widely used as aircraft materials. The use of global electrochemical techniques (OCP, PP, EIS) associated with morphological analyses allowed the assessment of the nature and evolution of the microgalvanic corrosion of uncoated and coated 7050-T7451 aluminium alloy.
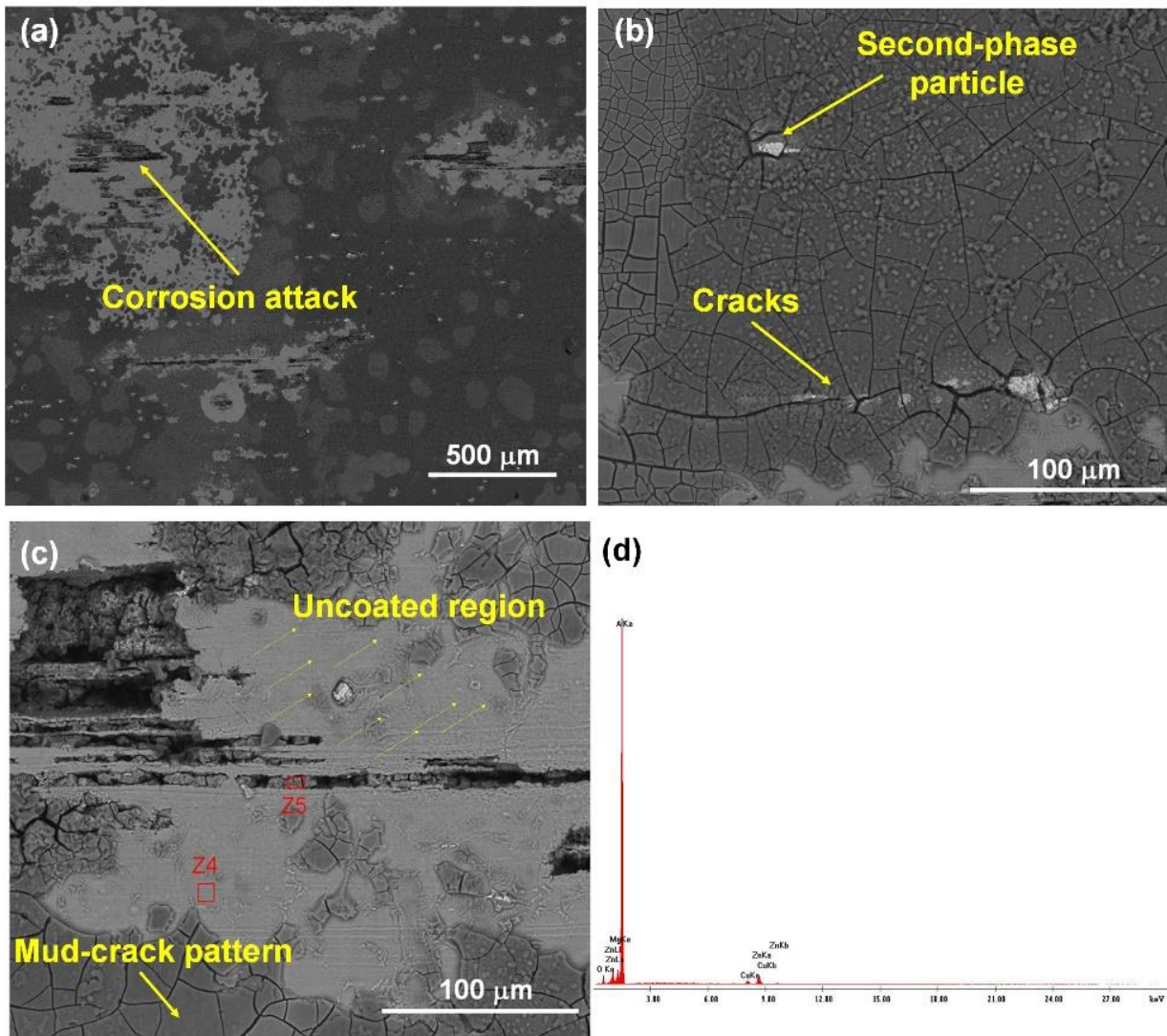

Figure 10. Surface morphology of the uncoated 7050-T7451 aluminium alloy after the EIS tests. **(a)** corrosive attack, **(b)** presence of second-phase particles and cracks, **(c)** mud-crack pattern and discovered region, and **(d)** EDX spectrum.
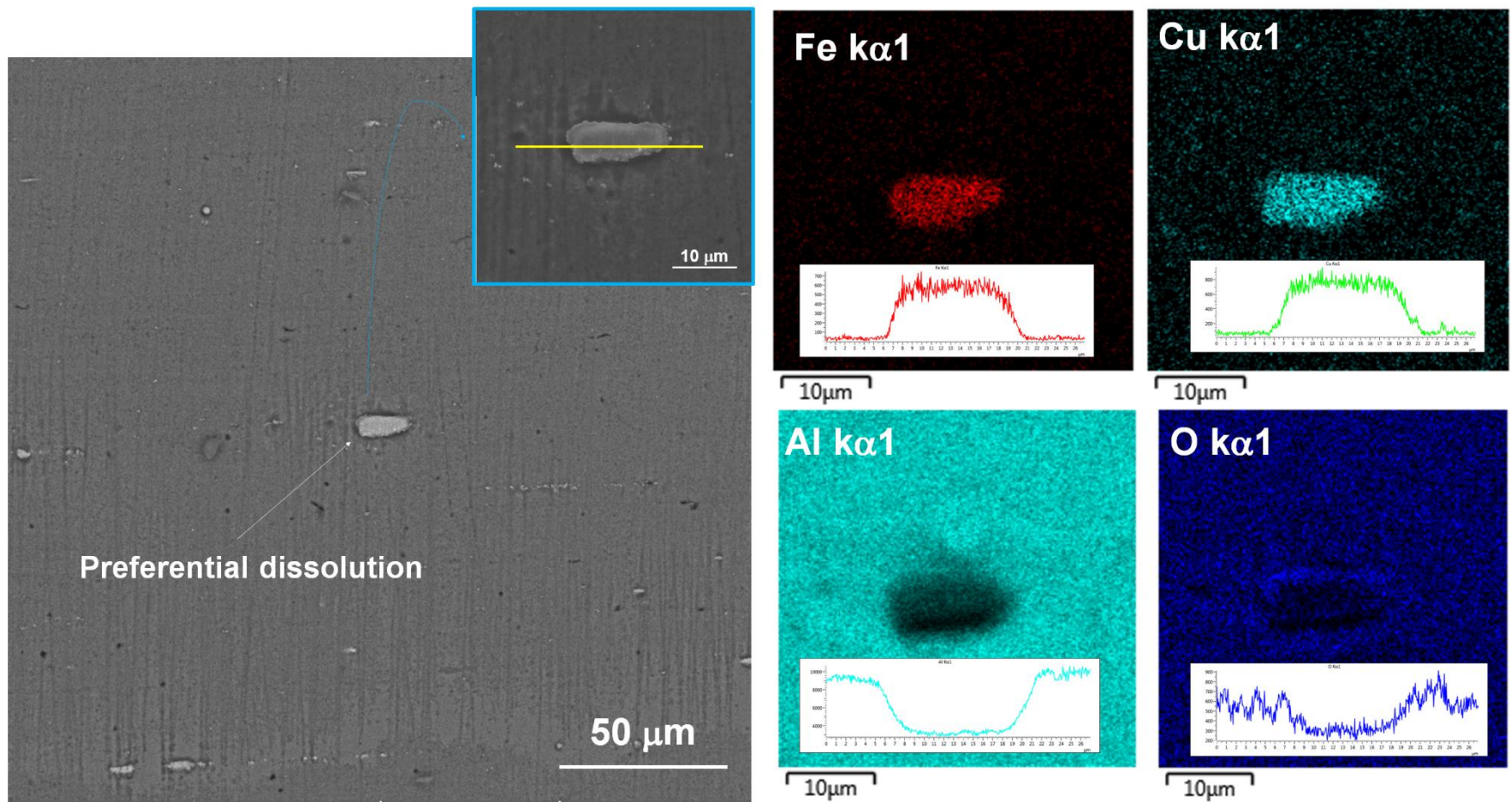
Figure 11. Presence of the second-phase particle on the 7050-T7451 aluminium matrix as well as the EDX results (maps and spectra).
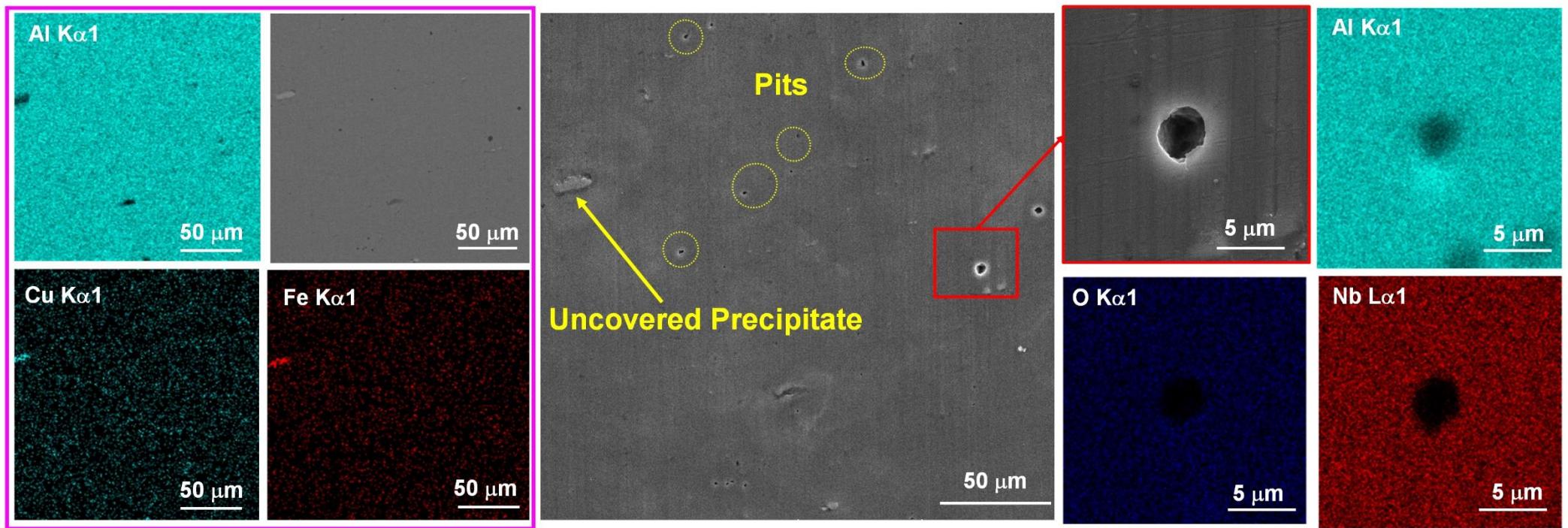
Figure 12. SEM images of the 7050-T7451 aluminium alloy containing Nb_2O_5 thin films after the EIS tests. The pink square (left side) represents the EDX concentration maps for the precipitate, which corresponds to the Al_7Cu_2Fe particle (52.10 Al, 7.37 Cu and 15.84 Fe atomic%). The square on the right side shows the EDX concentration maps for the pit.

4. Conclusions

This work verified the influence of Nb_2O_5 thin films deposited by using the reactive sputtering technique on global and localised corrosion processes of 7050-T74511 aluminium alloy in a medium containing an aggressive medium. The reactive sputtering technique was advantageous to produces Nb_2O_5 thin films on the 7050-T7451 aluminium alloy surface, presenting films with good adhesion and homogeneity. The produced Nb_2O_5 thin films acted as a protective barrier against corrosion process, improving the corrosion resistance of the 7050-T7451 aluminium alloy in an aggressive medium containing chloride ion. For uncoated aluminium alloy, the pitting potential ($E_{pitting}$) and corrosion potential (E_{corr}) are very close, leading the propagation of pitting on the corrosion potential. In contrast, in the present work it was created a safety margin between the $E_{pitting}$ and E_{corr} potentials about 315 mV, i.e., the reactive plasma treatment guarantees that the $E_{pitting}$ will not be attained. With respect to the EIS tests, the surface treatment increased the impedance moduli. Considering the coated material, the EIS spectra for the 96 h of immersion presented a better performance when compared to the base material (3 h of immersion). Considering the innovative technology developed, it envisaged the minimization of maintenance costs arising from the corrosion processes of the metallic materials as well as the competitiveness increasing by the aeronautical sector. From an economic point of view, the technological applications of niobium are of great importance for the Triângulo Mineiro region (Minas Gerais state - Brazil), where one of the world's largest reserves is located.

Conflict of interest
The authors declare that they have no known competing financial interests or personal relationships that could have appeared to influence the work reported in this paper.

Data availability
Not applicable

Code availability
Not applicable

Authors' contributions

Ferreira, M. O. A. – Investigation;

Teixeira, G. T. L. – Investigation;

Leite, N. B. - Formal analysis and writing-up;

Gelamo, R. V. – Investigation and Formal analysis;

Aoki, I. V. -   Formal analysis and revision

Pinto, H. C. – Formal analysis;

Moreto, J. A. – Project administration, Supervision, Investigation, Formal analysis, and writing-up;

6. References

[1]   L. Xu, X. Yu, L. Huy, S. Zhou, Fatigue life prediction of aviation aluminium alloy based on quantitative pre-corrosion damage analysis, Trans. Nonferrous Met. Soc. China 27 (2017) 1353–1362. https://doi.org/10.1016/S1003-6326(17)60156-0.

[2]   T. Sampath Kumar, A. Vinoth Jebaraj, Metallurgical characterization of CrN and AlCrN physical vapour deposition coatings on aluminium alloy AA 6061, Mater. Today Proc. 22 (2020) 1479–1488. https://doi.org/10.1016/J.MATPR.2020.01.506.

[3]   Z. Duan, C. Li, Y. Zhang, L. Dong, X. Bai, M. Yang, D. Jia, R. Li, H. Cao, X. Xu, Milling surface roughness for 7050 aluminum alloy cavity influenced by nozzle position of nanofluid minimum quantity lubrication, Chinese J. Aeronaut. 34 (2021) 33–53. https://doi.org/10.1016/J.CJA.2020.04.029.

[4]   J.A. Moreto, C.E.B. Marino, W.W. Bose Filho, L.A. Rocha, J.C.S. Fernandes, SVET, SKP and EIS study of the corrosion behaviour of high strength Al and Al–Li alloys used in aircraft fabrication, Corros. Sci. 84 (2014) 30–41. https://doi.org/10.1016/J.CORSCI.2014.03.001.

[5]   D. Yin, H. Liu, Y. Chen, D. Yi, B. Wang, B. Wang, F. Shen, S. Fu, C. Tang, S. Pan, Effect of grain size on fatigue-crack growth in 2524 aluminium alloy, Int. J. Fatigue. 84 (2016) 9–16. https://doi.org/10.1016/j.ijfatigue.2015.11.011.

[6]   M.L. de Bonfils-Lahovary, L. Laffont, C. Blanc, Characterization of intergranular corrosion defects in a 2024 T351 aluminium alloy, Corros. Sci. 119 (2017) 60–67. https://doi.org/10.1016/j.corsci.2017.02.020.

[7]   T. Aoba, M. Kobayashi, H. Miura, Effects of aging on mechanical properties and microstructure of multi-directionally forged 7075 aluminum alloy, Mater. Sci. Eng. A 700 (2017) 220–225. https://doi.org/10.1016/J.MSEA.2017.06.017.

[8]   A. Brotzu, G. de Lellis, F. Felli, D. Pilone, Study of defect formation in Al 7050 alloys, Procedia Struct. Integr. 3 (2017) 246–252. https://doi.org/10.1016/J.PROSTR.2017.04.015.

[9]   L.L. Liu, Q.L. Pan, X.D. Wang, S.W. Xiong, The effects of aging treatments on mechanical property and corrosion behavior of spray formed 7055 aluminium alloy, J. Alloys Compd. 735 (2018) 261–276. https://doi.org/10.1016/J.JALLCOM.2017.11.070.

[10] G. Ozer, A. Karaaslan, Properties of AA7075 aluminum alloy in aging and retrogression and reaging process, Trans. Nonferrous Met. Soc. China 27 (2017) 2357–2362. https://doi.org/10.1016/S1003-6326(17)60261-9.

[11] J. Li, F. Li, X. Ma, J. Li, S. Liang, Effect of grain boundary characteristic on intergranular corrosion and mechanical properties of severely sheared Al-Zn-Mg-Cu alloy, Mater. Sci. Eng. A 732 (2018) 53–62. https://doi.org/10.1016/J.MSEA.2018.06.097.

[12] F.X. Song, X.M. Zhang, S.D. Liu, Q. Tan, D.F. Li, Exfoliation corrosion behavior of 7050-T6 aluminum alloy treated with various quench transfer time, Trans. Nonferrous Met. Soc. China 24 (2014) 2258–2265. https://doi.org/10.1016/S1003-6326(14)63342-2.

[13] J. Zhao, Y. Deng, J. Tang, J. Zhang, Effect of gradient grain structures on corrosion resistance of extruded Al–Zn–Mg–Cu alloy, J. Alloys Compd. 832 (2020) 154911. https://doi.org/10.1016/J.JALLCOM.2020.154911.

[14] Y.C. Lin, J.L. Zhang, G. Liu, Y.J. Liang, Effects of pre-treatments on aging precipitates and corrosion resistance of a creep-aged Al–Zn–Mg–Cu alloy, Mater. Des. 83 (2015) 866–875. https://doi.org/10.1016/J.MATDES.2015.06.029.

[15] F.X. Song, X.M. Zhang, S.D. Liu, N.M. Han, D.F. Li, Anisotropy of localized corrosion in 7050-T7451 Al alloy thick plate, Trans. Nonferrous Met. Soc. China 23 (2013) 2483–2490. https://doi.org/10.1016/S1003-6326(13)62758-2.

[16] W. Hou, W. Ji, Z. Zhang, J. Xie, X. Cheng, The effect of homogenization temperature on the corrosion resistance of extruded 7050 Al-alloy bars, J. Mater. Process Technol. 214 (2014) 635–640. https://doi.org/10.1016/J.JMATPROTEC.2013.11.009.

[17] F. Song, X. Zhang, S. Liu, Q. Tan, D. Li, The effect of quench rate and over ageing temper on the corrosion behaviour of AA7050, Corros. Sci. 78 (2014) 276–286. https://doi.org/10.1016/J.CORSCI.2013.10.010.

[18] J. Chen, X. Zhang, L. Zou, Y. Yu, Q. Li, Effect of precipitate state on the stress corrosion behavior of 7050 aluminum alloy, Mater. Charact. 114 (2016) 1–8. https://doi.org/10.1016/J.MATCHAR.2016.01.022.

[19] C. Mondal, A.K. Mukhopadhyay, On the nature of T(Al2Mg3Zn3) and S(Al2CuMg) phases present in as-cast and annealed 7055 aluminum alloy, Mater. Sci. Eng. A 391 (2005) 367–376. https://doi.org/10.1016/J.MSEA.2004.09.013.

[20] M. Yu, H. Zu, K. Zhao, J. Liu, S. Li, Effects of dry/wet ratio and pre-immersion on stress corrosion cracking of 7050-T7451 aluminum alloy under wet-dry cyclic conditions, Chinese J. Aeronaut. 31 (2018) 2176–2184. https://doi.org/10.1016/J.CJA.2018.01.008.

[21] Y. Sun, Q. Pan, Y. Sun, W. Wang, Z. Huang, X. Wang, Q. Hu, Localized corrosion behavior associated with Al_7Cu_2Fe intermetallic in Al-Zn-Mg-Cu-Zr alloy, J. Alloys Compd. 783 (2019) 329–340. https://doi.org/10.1016/J.JALLCOM.2018.12.151.

[22] A. Chemin, D. Marques, L. Bisanha, A. de J. Motheo, W.W. Bose Filho, C.O.F. Ruchert, Influence of Al_7Cu_2Fe intermetallic particles on the localized corrosion of high strength aluminum alloys, Mater. Des. 53 (2014) 118–123. https://doi.org/10.1016/J.MATDES.2013.07.003.

[23] Z. Wang, H. Jiang, H. Li, S. Li, Effect of solution-treating temperature on the intergranular corrosion of a peak-aged Al-Zn-Mg-Cu alloy, J. Mater. Res. Technol. 9 (2020) 6497–6511. https://doi.org/10.1016/j.jmrt.2020.04.035.

[24] J.A. Moreto, O. Gamboni, C.O.F.T. Ruchert, F. Romagnoli, M.F. Moreira, F. Beneduce, W.W. Bose Filho, Corrosion and fatigue behavior of new Al alloys, Procedia Eng. 10 (2011) 1521–1526. https://doi.org/10.1016/J.PROENG.2011.04.254.

[25] E. Cadoni, M. Dotta, D. Forni, H. Kaufmann, Effects of strain rate on mechanical properties in tension of a commercial aluminium alloy used in armour applications, Procedia Struct. Integr. 2 (2016) 986–993. https://doi.org/10.1016/J.PROSTR.2016.06.126.

[26] Y. Ma, H. Wu, X. Zhou, K. Li, Y. Liao, Z. Liang, L. Liu, Corrosion behavior of anodized Al-Cu-Li alloy: The role of intermetallic particle-introduced film defects, Corros. Sci. 158 (2019) 108110. https://doi.org/10.1016/J.CORSCI.2019.108110.

[27] G. Hu, C. Zhu, D. Xu, P. Dong, K. Chen, Effect of cerium on microstructure, mechanical properties and corrosion properties of Al-Zn-Mg alloy, J. Rare Earths 39 (2021) 208–216. https://doi.org/10.1016/J.JRE.2020.07.010.

[28] R.G. Toro, P. Calandra, B. Cortese, T. de Caro, M. Brucale, A. Mezzi, F. Federici, D. Caschera, Argon and hydrogen plasma influence on the protective properties of diamond-like carbon films as barrier coating, Surf. Interfaces 6 (2017) 60–71. https://doi.org/10.1016/J.SURFIN.2016.11.009.

[29] A. Modabberasl, M. Sharifi, F. Shahbazi, P. Kameli, Multifractal analysis of DLC thin films deposited by pulsed laser deposition, Appl. Surf. Sci. 479 (2019) 639–645. https://doi.org/10.1016/J.APSUSC.2019.02.062.

[30] J. Chen, P. Ji, Y. Yang, C. Jin, L. Zhuge, X. Wu, The structure and properties of amorphous diamond-like carbon films deposited by helicon wave plasma chemical vapor deposition, Thin Solid Films 709 (2020) 138167. https://doi.org/10.1016/J.TSF.2020.138167.

[31] H. Maruno, A. Nishimoto, Adhesion and durability of multi-interlayered diamond-like carbon films deposited on aluminum alloy, Surf. Coat. Technol. 354 (2018) 134–144. https://doi.org/10.1016/J.SURFCOAT.2018.08.094.

[32] L.R. Freitas, R.V. Gelamo, C.E.B. Marino, J.P.L. Nascimento, J.M.A. Figueiredo, J.C.S. Fernandes, J.A. Moreto, Corrosion behaviour of reactive sputtering deposition niobium oxide-based coating on the 2198-T851 aluminium alloy, Surf. Coat. Technol. 434 (2022) 128197. https://doi.org/10.1016/J.SURFCOAT.2022.128197.

[33] M.O.A. Ferreira, R.V. Gelamo, C.E.B. Marino, B.P. da Silva, I.V. Aoki, M.S. da Luz, N.D. Alexopoulos, N.B. Leite, J.A. Moreto, Effect of niobium oxide thin film on the long-term immersion corrosion of the 2198-T851 aluminium alloy, Materialia 22 (2022) 101407. https://doi.org/10.1016/J.MTLA.2022.101407.

[34] J.P.L. do Nascimento, M.O.A. Ferreira, R.V. Gelamo, J. Scarmínio, T.T. Steffen, B.P. da Silva, I.V. Aoki, A.G. dos Santos, V.V. de Castro, C. de Fraga Malfatti, J.A. Moreto, Enhancing the corrosion protection of Ti-6Al-4V alloy through reactive sputtering niobium oxide thin films, Surf. Coat. Technol. 428 (2021) 127854. https://doi.org/10.1016/J.SURFCOAT.2021.127854.

[35] J.A. Moreto, R.V. Gelamo, J.P.L. Nascimento, M. Taryba, J.C.S. Fernandes, Improving the corrosion protection of 2524-T3-Al alloy through reactive sputtering Nb_2O_5 coatings, Appl. Surf. Sci. 556 (2021) 149750. https://doi.org/10.1016/J.APSUSC.2021.149750.

[36] M.C. de Almeida Bino, W.A. Eurídice, R.V. Gelamo, N.B. Leite, M.V. da Silva, A. de Siervo, M.R. Pinto, P.A. de Almeida Buranello, J.A. Moreto, Structural and morphological characterization of Ti-6Al-4V alloy surface functionalization based on Nb_2O_5 thin film for biomedical applications, Appl. Surf. Sci. 557 (2021) 149739. https://doi.org/10.1016/J.APSUSC.2021.149739.

[37] J.A. Moreto, R.V. Gelamo, M.V. da Silva, T.T. Steffen, C.J.F. de Oliveira, P.A. de Almeida Buranello, M.R. Pinto, New insights of Nb_2O_5-based coatings on the 316L SS surfaces: enhanced biological responses, J. Mater. Sci. Mater. Med. 32 (2021) 25. https://doi.org/10.1007/s10856-021-06498-7.

[38] G. Ramírez, S.E. Rodil, S. Muhl, D. Turcio-Ortega, J.J. Olaya, M. Rivera, E. Camps, L. Escobar-Alarcón, Amorphous niobium oxide thin films, J. Non. Cryst. Solids 356 (2010) 2714–2721. https://doi.org/10.1016/J.JNONCRYSOL.2010.09.073.

[39] M.F. Pillis, M.C.L. de Oliveira, R.A. Antunes, Surface chemistry and the corrosion behavior of magnetron sputtered niobium oxide films in sulfuric acid solution, Appl. Surf. Sci. 462 (2018) 344–352. https://doi.org/10.1016/J.APSUSC.2018.08.123.

[40] F. Mansfeld, J.C.S. Fernandes, Impedance spectra for aluminum 7075 during the early stages of immersion in sodium chloride, Corros. Sci. 34 (1993) 2105–2108. https://doi.org/10.1016/0010-938X(93)90063-M.

[41] K. Jüttner, Electrochemical Impedance Spectroscopy (EIS) of corrosion processes on inhomogeneous surfaces, Electrochim. Acta 35 (1990) 1501.

[42] M.W. Kendig, F. Mansfeld, AC electrochemical impedance of a model pit, J. Electrochem. Soc. 129 (1982). C318-C318.

[43] D.L. Ferreira, E.M. Alves, G.R. Sousa, P.H.B. Ferreira, J.M.A. Figueiredo, N.B. Leite, J.A. Moreto, Electrochemical impedance spectroscopy: basic principles and some applications, Rev. Virtual Quim. (2022) 1-17. http://dx.doi.org/10.21577/1984-6835.20220114.

[44] C.A.R. Maestro, J.A. Moreto, T. Chiaramonte, R.V. Gelamo, C.J.F. de Oliveira, M.M. Santos, M.V. da Silva, A.H.S. Bueno, R.M. Balestra, A.M.S. Mafafaia, Corrosion behavior and biological responses of a double coating formed on the Ti-6Al-4V alloy surface by using thermal oxidation and biomimetic deposition of bismuth-doped CaP, Surf. Coat. Technol. 425 (2021) 127717. https://doi.org/10.1016/j.surfcoat.2021.127717.

[45] J.A. Moreto, M.S. dos Santos, M.O.A. Ferreira, G.S. Carvalho, R.V. Gelamo, I.V. Aoki, M. Taryba, W.W. Bose Filho, J.C.S. Fernandes, Corrosion and corrosion-fatigue synergism on the base metal and nugget zone of the 2524-T3 Al alloy joined by FSW process, Corros. Sci., 182 (2021) 109253. https://doi.org/10.1016/j.corsci.2021.109253.

[46] G.J. Brug, A.L.G. van den Eeden, M. Sluyters-Rehbach, J.H. Sluyters, The analysis of electrode impedances complicated by the presence of a constant phase element. J. Electroanal. Chem. Interfacial Electrochem. 176 (1984) 275-295. https://doi.org/10.1016/S0022-0728(84)80324-1.

[47] B. Hirschorn, M.E. Orazem, B. Tribollet, V. Vivier, I. Frateur, M. Musiani, Constant-phase-element behavior caused by resistivity distributions in films: Theory, J. Electrochem. Soc. 157 (2010) C452.https://doi.org/10.1149/1.3499564.

[48] M. Orazem, B. Tribollet, Electrochemical Impedance Spectroscopy, second ed., John Wiley & Sons, Inc, New Jersey 2017.

[49] F.J. Martin, G.T. Cheek, W.E. O'Grady, P.M. Natishan, Impedance studies of the passive film on aluminium, Corros. Sci. 47 (2005) 3187-3201. https://doi.org/10.1016/j.corsci.2005.05.058.

[50] S. Clima, G. Pourtois, S. van Elshocht, S. de Gendt, M.M. Heyns, D.J. Wouters, J.A. Kittl, Dielectric Response of Ta_2O_5, $NbTaO_5$ and Nb_2O_5 from First-Principles Investigations, ECS Transactions. 19 (2019) 729–737. https://doi.org/10.1149/1.3122128.

[51] K.A. Yasakau, M.L. Zheludkevich, S.V. Lamaka, M.G.S. Ferreira, Role of intermetallic phases in localised corrosion of AA5083, Electrochim. Acta 52 (2007) 7651–7659. https://doi.org/10.1016/j.electacta.2006.12.072.

[52] Q. Meng, G.S. Frankel, Effect of Cu content on corrosion behaviour of 7xxx series aluminium alloys. J. Electrochem. Soc. 151 (2004) B271–B283. https://doi.org/ 10.1149/1.1695385.

[53] J.R. Davis, Corrosion of Aluminium and Aluminium Alloys, first ed. ASM International, Materials Park, 1999.

[54] N. Birbilis, R.G. Buchheit, Investigation and discussion of characteristics for intermetallic phases common to aluminium alloys as a function of solution pH. J. Electrochem. Soc. 155 (2008) C117–C126. https://doi.org/ 10.1149/1.2829897.

[55] N. Birbilis, R.G. Buchheit, Electrochemical characteristics of intermetallic phases in aluminium alloys: an experimental survey and discussion. J. Electrochem. Soc. 152 (2005) B140–B151, https://doi.org/10.1149/1.1869984.